Electron Microscopy of the "Disordered Phase" in Nb-Ge Thin Films

M. ARITA

College of General Education, Nagoya University, Nagoya, 464, Japan

AND H.-U. NISSEN

Solid State Physics Laboratory, Swiss Federal Institute of Technology (ETH), CH-8093 Zürich, Switzerland

Thin films of Nb–Ge textures contain regions of highly disordered Nb–Ge, the precise atomic structure of which has previously not been resolved. A detailed selected area electron diffraction investigation involving tilt series around many differently oriented axes, as well as high resolution electron microscopy, allows the interpretation of these regions as assemblies of grains with a strongly defective crystal structure, and some regions giving amorphous-like contrasts in the electron micrographs. The crystalline regions have been identified possibly as orthorhombic with $a = 0.85$ nm, $b = 0.67$ nm, and $c = 0.35$ nm. The grain boundaries, planar defects, and lattice distortions in the crystalline grains are described. The texture of these grains, together with the possibly amorphous component, causes the complicated "streaked" electron diffraction patterns which can be obtained for any orientation of the electron beam. © 1993 Academic Press, Inc.

Introduction

In recent research on crystalline superconductor materials, transmission electron microscope (TEM) studies, together with selected area diffraction (SAD) investigations, have gained an increasing importance for elucidating the relations between the crystallographic microstructures (texture and defect structure) of such materials and their physical (especially superconductor) properties. The defect structure includes the arrangement of local chemical variations such as chemical domains, voids, superstructures, and chemical inhomogeneities at grain and phase boundaries. These studies have been executed with equal intensity on the new high-T_c superconductors (for example (1–3)) and on the classical superconductor materials such as Nb_3Sn and Nb_3Ge thin films (for example (4, 5)). They have also been successful for the elucidation of extremely fine-grained superconductor material, like NbN and other refractory compounds, where other single crystal diffraction techniques cannot easily be applied.

Nb–Ge superconductor films synthesized by sputtering techniques, chemical vapor deposition, or evaporation are generally polycrystalline and contain a variety of crystal phases with different kinds and amounts of defects. Besides the superconducting Nb_3Ge phase with the cubic A15 structure, other minority phases like Nb_5Ge_3 with the tetragonal $D8_m$ structure and also with hexagonal $D8_g$-structure have been identified and reported to be either stable or metastable phases (6–8). The amount of these additional phases can be varied by changing the film preparation parameters, e.g., deposition rate and temperature.

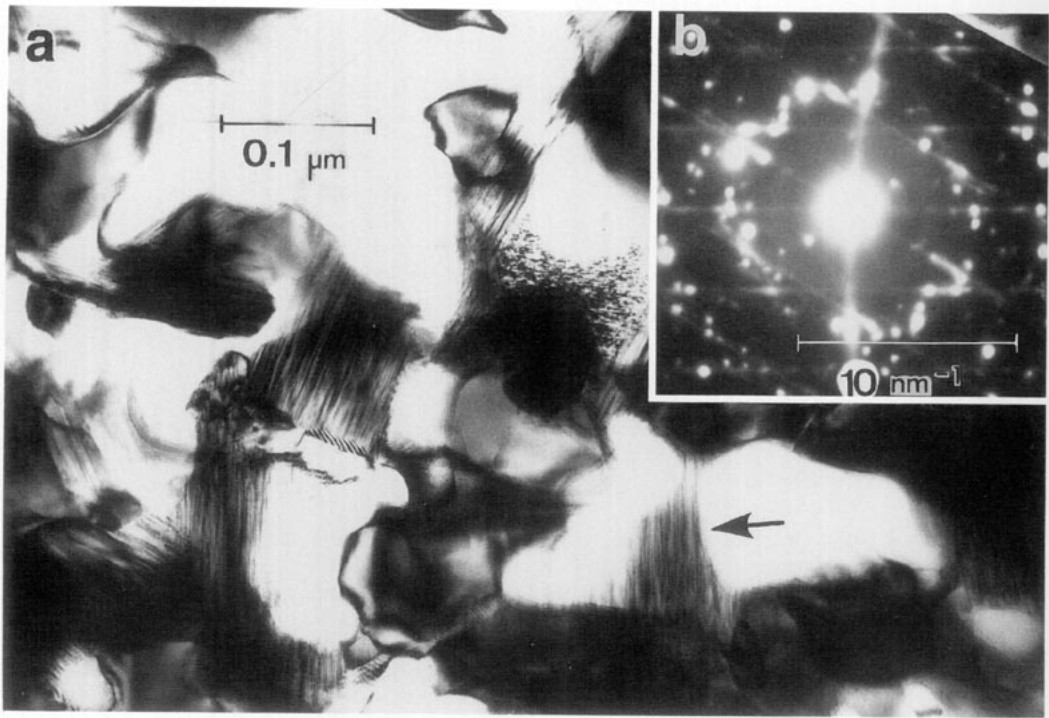For most of these phases, precise crystallographic data have been obtained by SAD

FIG. 1. (a) Typical bright field image of a region in texture occupied by the "disordered phase." One example of the "disordered phase" is indicated by an arrow. (b) Corresponding electron diffractogram. Streaks with different orientations are recognized.

studies combined with X-ray diffraction investigations. On the other hand, for a few components of these films, especially for certain regions that exhibit lamellar contrast in the electron micrographs, the precise crystallographic determination was impossible due to unusual irregular contrast features previously attributed to some form of structural disorder (5, 9–14). In this study, regions with lamellar contrast will be referred to as the "disordered phase." The aim of this paper is to elucidate the structural state, the type, and amount of disorder, as well as any determinable crystallographic parameters of the components of the "disordered phase" by using SAD and high resolution transmission electron microscopy (HRTEM).

An example of a region in the texture occupied by the "disordered phase" is shown in Fig. 1a, and a typical strongly streaked

SAD pattern is presented in Fig. 1b. By measuring the positions of intensity maxima within the diffraction streaks, Cullis et al. (9) reported that the "disordered phase" is Nb_5Ge_3 having the $D8_m$ structure. By contrast, Païdassi (10) associated this material with the $D8_8$-structure on the basis of his SAD work and, finally, Kitano et al. (5) suggested a mixture of different niobium oxides as a possible explanation. In view of these findings, the chemical nature of the "disordered phase" remains obscure. The present study therefore aims to classify both the structure and the chemical composition of the "disordered phase."

2. Experimental Procedure

Nb–Ge tapes were prepared by the coevaporation method using pure Nb (MARZ grade, Material Research Corp.) and pure

Ge (99.999%, semiconductor purity). After the evacuation down to the order of 10^{-6} Pa ($\approx 10^{-8}$ Torr), the evaporation was started. Vapors of these elements were deposited onto molybdenum polycrystalline substrates kept at about 1.12×10^3 K ($\approx 850°$C). The vacuum during the deposition was about twice as bad as the value before the evaporation started. Details of the method are presented in references (*13, 15, 16*).

For the electron microscopy, the Nb–Ge tapes were chemically etched using the method developed by Yin *et al.* (*11*) and Yin and Schauer (*17*). Observations were performed in a JEOL JEM 100C electron microscope equipped with a double tilt goniometer ($\pm 60°$) or a JEOL JEM 200CX electron microscope equipped with a top entry tilting goniometer (THG-2; $\pm 10°$, $C_s = 1.2$ mm, point resolution of 0.24 nm). For the high resolution images only diffraction spots with space frequencies smaller than 4.3 nm^{-1} were allowed to contribute to the image. The camera lengths of the SAD patterns were accurately measured using a polycrystalline gold foil. The magnifications of the optical diffraction (OD) patterns from the HRTEM images of the "disordered phase" were estimated using OD patterns from adjacent A15 images.

In order to investigate the local chemical composition of the "disordered phase," energy dispersive X-ray spectroscopy (EDS) was performed using a Tracor Northern EDS system mounted on a Philips EM430 microscope operated at 300 kV. The spot size of the electron beam was about 10–20 nm in diameter. It was assumed that the specimen was sufficiently thin to allow the use of the thin film approximation.

3. Results and Discussion

3.1. Size Distribution and X-Ray Microanalysis

In order to obtain information about the germanium concentration of the "disordered phase," the amount of this phase was compared for different specimens. This was
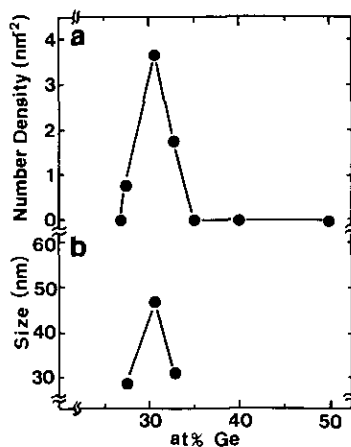

FIG. 2. (a) Number density and (b) average size of "disordered phase" against the germanium concentration.

necessary since their amount and average size vary as a function of the average volume fraction, and because the Ge-content of this volume fraction can influence the average Ge-content of the entire film. The sizes, defined as the square root values of the area, varied between 10 nm and 100 nm as reported earlier (*5*). In Fig. 2, the number density (i.e., the number per unit area) as well as the size in nm of the "disordered phase" are plotted against the measured Ge contents (in at.%) for seven Nb–Ge films. Figure 2 shows that both parameters plotted in this figure have maximum values at approximately 30 at.% Ge.

Together with the TEM investigation, X-ray microanalytical determination of Nb and Ge were made on two regions containing the lamellar contrast in a specimen with a bulk Ge-content of 30.6 at.% (the T_c-values for this specimen were 17.27–14.42 K). Assuming that these two regions contained only Nb and Ge, their respective Ge-content were 27.0 and 28.1 at.%. The adjacent crystal grains of A15 material were also measured for comparison and gave 24.6 and 25.9 at.% Ge, respectively. From these two independent sets of measurements it may be concluded, as a rough approximation, that

the "disordered phase" contains about 30 ± 5 at.% Ge.

3.2. Structure Characteristics

In Fig. 3, a typical high resolution lattice image of a "disordered phase" is shown together with its laser optical diffractograms (OD). Images of this type have also been presented by Kitano et al. (5). The d-value which corresponds to the distance between two adjacent streaks is 0.31 nm, and the periodicity along the streak is 0.85 nm. In a similar way, OD were made from 13 TEM images of this type. Some of them were the same as Fig. 3, and the others showed different patterns. This is due to the different observation directions used. The largest d-values obtained from the distances between two adjacent streaks in these patterns was about 0.35 nm.

Figure 4a presents a SAD pattern showing virtually the same pattern as the OD in Fig. 3. When this pattern was rotated around the direction of the streak, the distance between the streaks increased gradually (Figs. 4b–4g). The streaks also take on a curvature that is due to the influence of the edge of the Ewald sphere. Finally, in Figs. 4h and 4i, spotty patterns were obtained. These patterns also contained weak and fine streaks along the directions of the arrows (These "fine streaks" can be more clearly recognized in Fig. 6). In the corresponding bright field images (Fig. 5), the lamellar contrast was visible at smaller rotation angles. The contrast changed gradually as the rotation angle was increased, and finally a mottled contrast was obtained, Fig. 5i.

Using another "disordered phase," a similar investigation of rotation was performed (Fig. 6). While the rotation axis in Fig. 4 was inclined by about 32° from the "fine streaks," they were nearly parallel or perpendicular to the "fine streaks" respectively in Figs. 6a and 6b. The same pattern as Fig. 4i is presented in Figs. 6a-A and 6b-C. The hexagons in these figures correspond to that in Fig. 4i. In this case also, the aperture size for SAD is larger than the size of the

"disordered phase," thus the diffraction spots and streaks from the neighboring area are superimposed. Streaks from the "disordered phase" presently considered are indicated by arrows. In both rotation series, circular patterns containing "fine streaks" with intensity maxima are seen after rotation by small angle. Further rotation gives patterns with less curvature, and the adjacent streaks become observable. Gradually, the distances between the streaks decreases as demonstrated in Fig. 4. In these cases, also, irregular lamellar contrasts were observed in TEM images after rotation by relatively large angles.

In all rotation series around three different axes (Figs. 4, 6a, and 6b), the distance between streaks gradually changed as a function of the rotation angle. No regular intensity distributions were recognized between the streaks. Thus, it is assumed that the "disordered phase" has intensity distribution only on the streaks in the SAD patterns. Based on these results, the intensity distribution in three-dimension must have a layer structure shown in Fig. 7, which is oriented along the incident beam direction of Figs. 4i, 6a-A, and 6b-C (arrow in Fig. 7). The layers may contain spots and "fine streaks." They must contain also diffuse intensity which fills the rest of the area in the layer. Otherwise, it cannot be explained that the streaks were obtained by any rotation investigated. From the rotation angles and the distances between the streaks of several SAD patterns, the distance between the layers in the reciprocal space was obtained. The value estimated using Fig. 4 was 2.83 ± 0.02 nm^{-1} (d-value: 0.353 ± 0.002 nm) as indicated in Fig. 7.

Under the assumption of the layer structure in the reciprocal space, the intensity distribution on the 0th layer is directly studied in Figs. 4i, 6a-A, or 6b-C. Since the intensity distribution around the center beam cannot be clearly seen in these three figures, Fig. 6a-B is magnified in Fig. 8 instead, where the observation direction is very near to that of Fig. 6a-A. In this figure, two sets
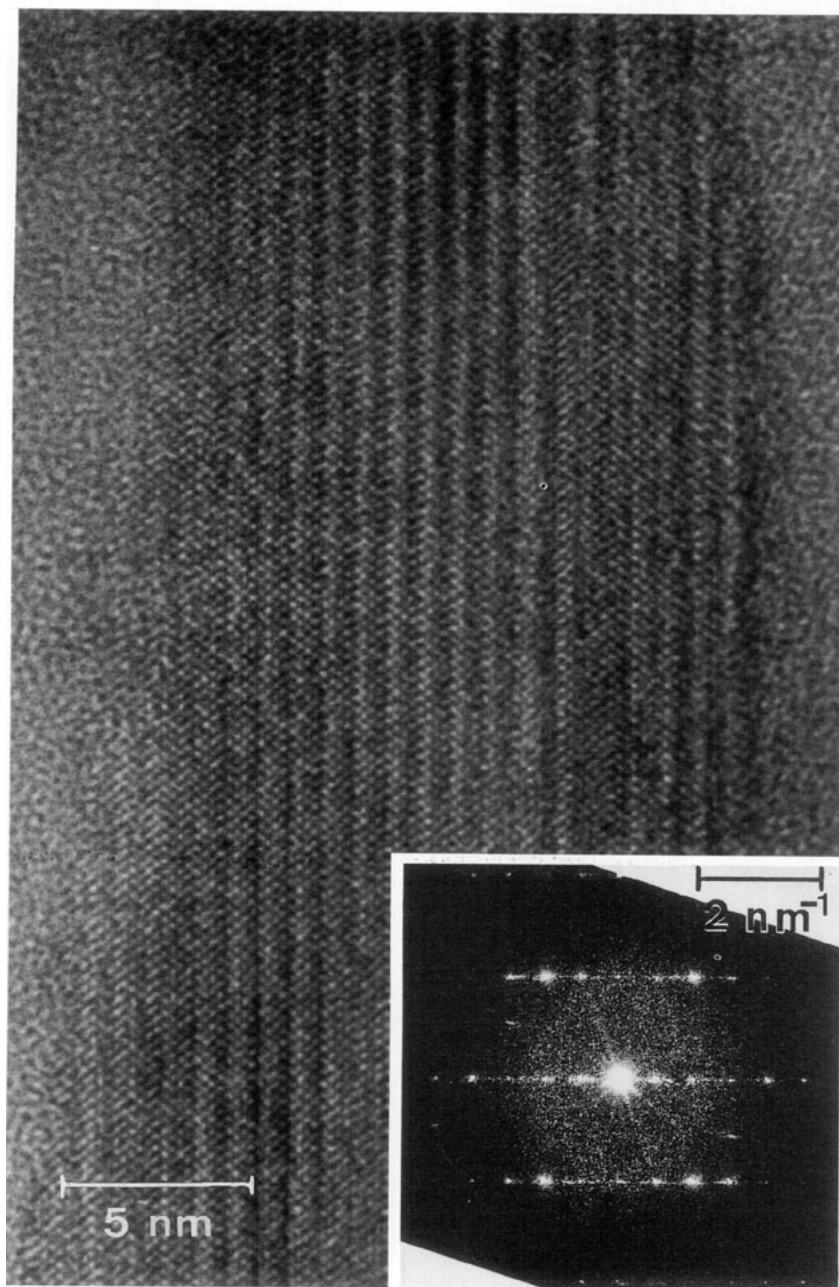
FIG. 3. Typical HRTEM image of a "disordered phase" observed from a certain direction. Its laser optical diffractogram is inserted.

of rectangular nets connecting diffraction spots are recognized. They are indicated by full or broken lines, respectively. The size of the rectangular nets are the same as each other. Thus, it is expected the "disordered phase" contains crystal lattices with different orientations. In addition, "fine streaks" marked by arrows are along the horizontal
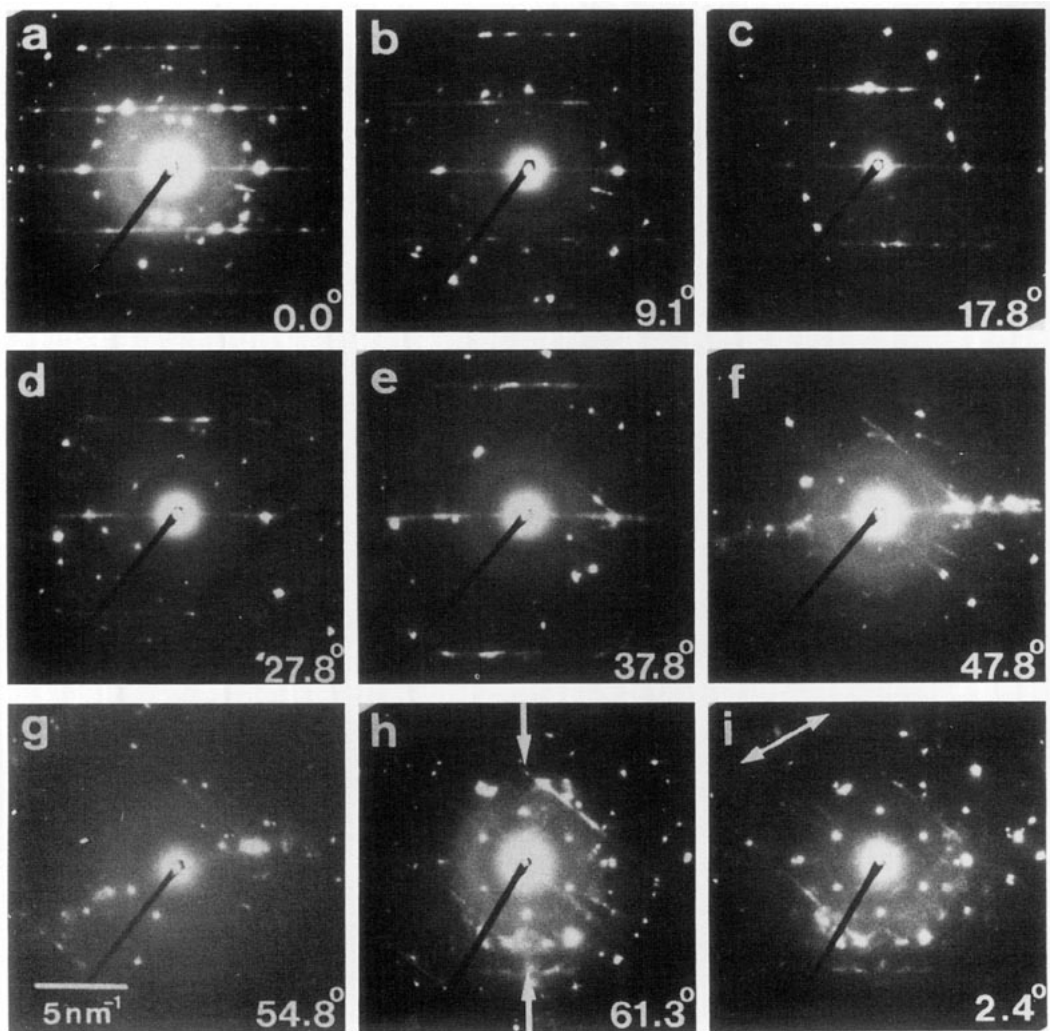
FIG. 4. Electron diffraction patterns after a rotation around a direction nearly parallel to the streak. (a) is the same pattern as the optical diffractogram in Fig. 3. The rotation angle is given in each figure. Since the rotation axis deviated slightly from the streak, (h) is not in perfect axial condition. Therefore, the reciprocal lattice was rotated 2° around the arrow direction in (h). Resulting pattern (i) contains very weak and fine streaks along the arrow.

direction in the figure. The other spots and streaks are assumed as the contribution from the adjacent grains.

Figure 9 is a high resolution image of a "disordered phase" used in Fig. 6, yielding the SAD pattern of Fig. 6a-A. The area within the circle marked by A in Fig. 9a is magnified in Fig. 9b. The "disordered phase" is an assembly of small crystal grains which show the characteristic rectangle cross-fringe contrast. Using arrows indicating the longer edges of the rectangular contrast, two lattice orientations can be recognized, which are rotated by approximately 60° against each other in the image plane. Figures 9c-A–9c-E are OD patterns from the circles A to E of Fig. 9a, respectively. Hexagonal patterns with "fine streaks" which are similar to the SAD patterns in Figs. 4i, 6a-A, or 6b-C were obtained from
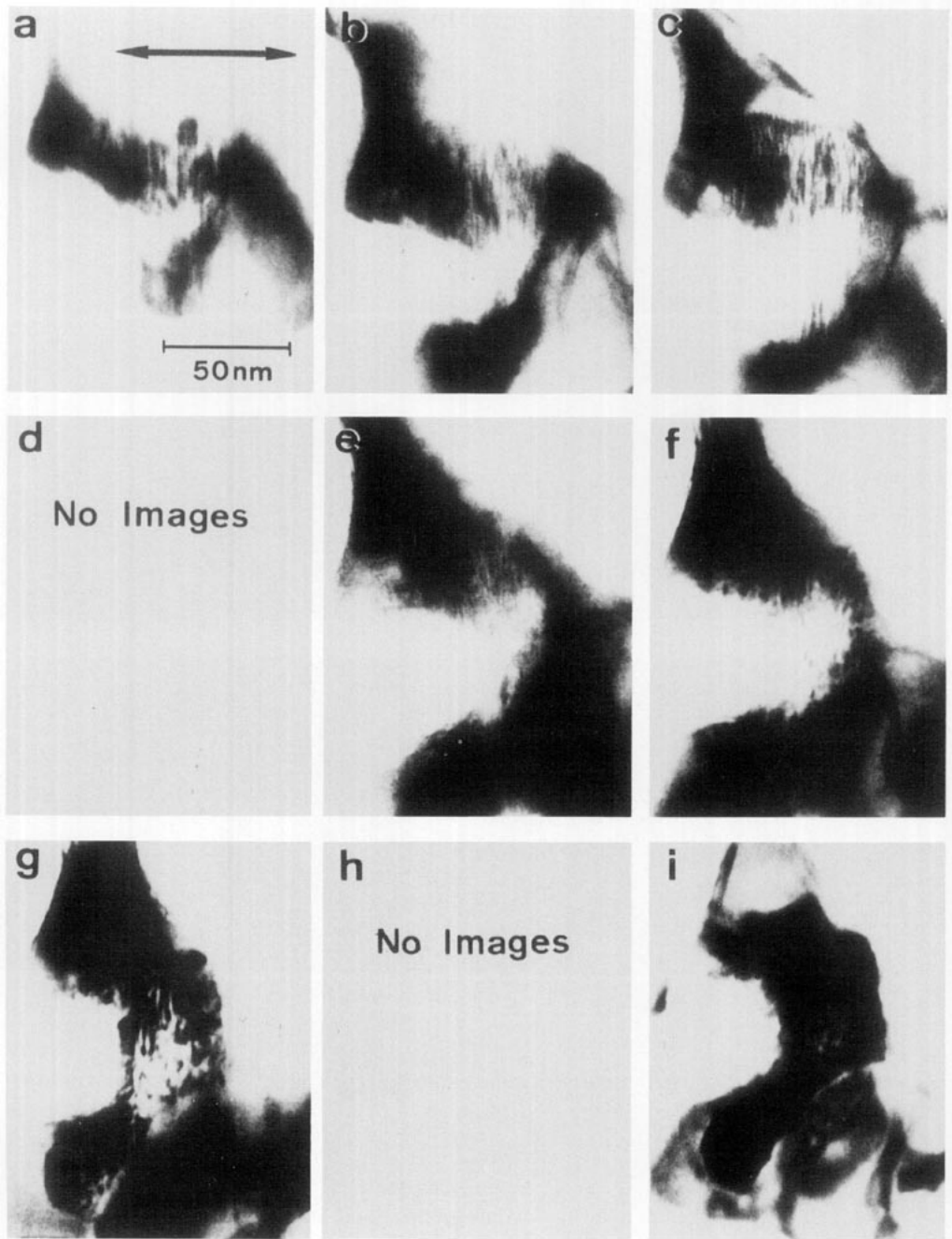
FIG. 5. Bright field image of the "disordered phase" used for Fig. 4. The rotation axis is indicated by an arrow in (a). (a)–(i) correspond to Figs. 4a–4i, respectively. The characteristic lamellar contrast is recognized in the images with small rotation angles.
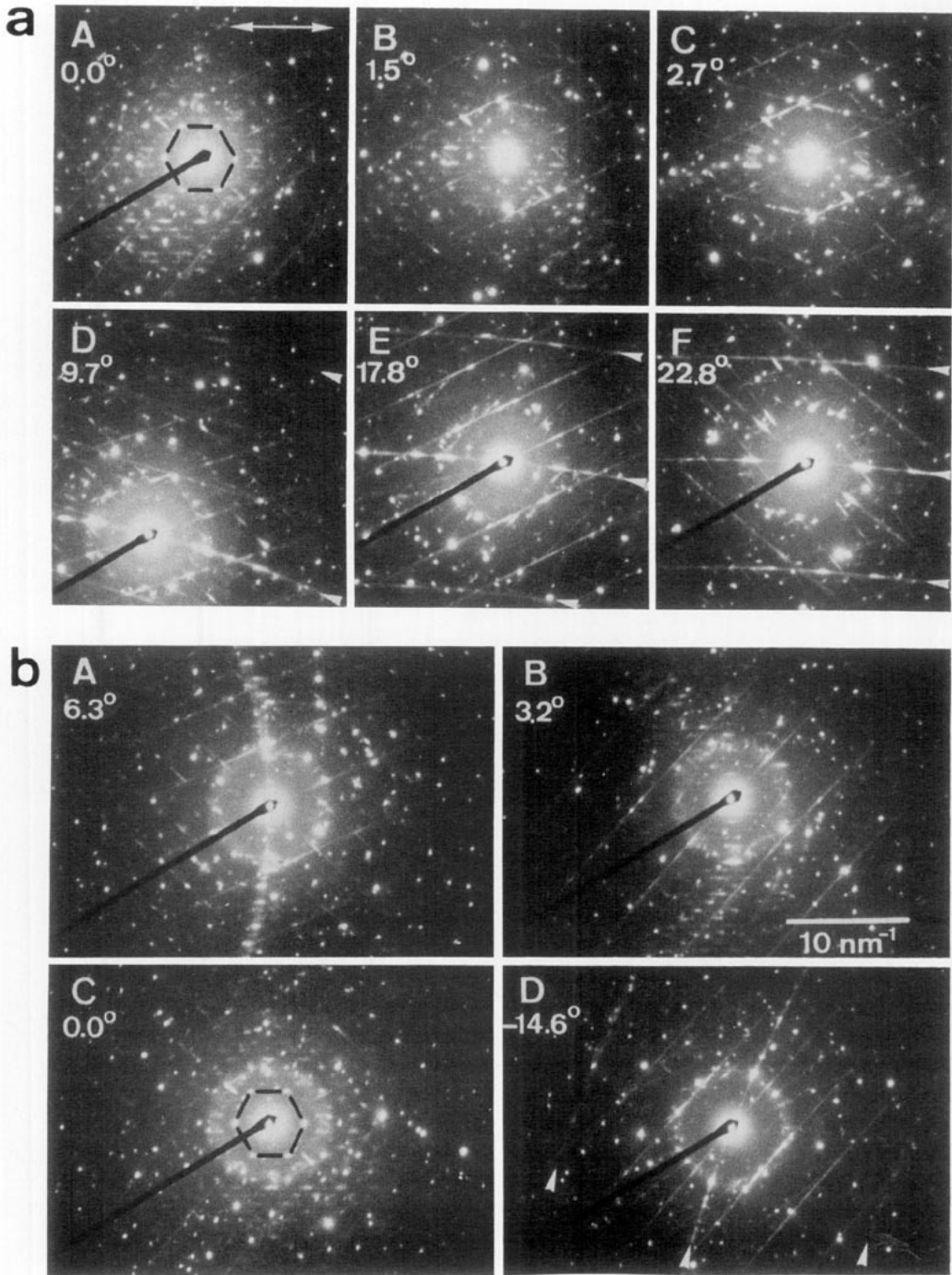
FIG. 6. Electron diffraction patterns after a rotation around directions (a) nearly parallel and (b) nearly perpendicular to the "fine streaks." The "fine streaks" are along the direction indicated by arrows in (a-A). The rotation angle is given in each figure. For example in (a-F), the streaks which are not along the horizontal direction are from adjacent "disordered phase." For clarity, streaks from the "disordered phase" discussed are marked by small arrows.
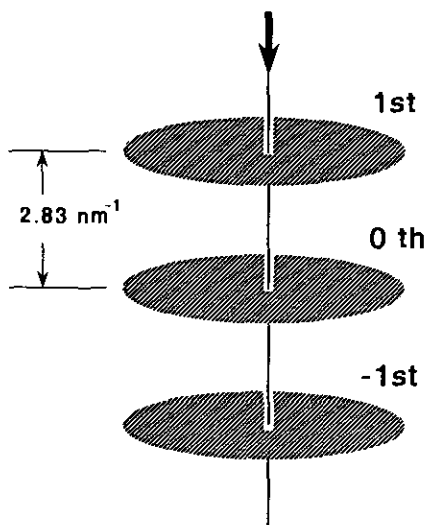
FIG. 7. A reciprocal space model of the "disordered phase." In the model, intensity is distributed on the layers, and no intensity is present between the layers. The layers may contain spots, "fine streaks" with intensity maxima as well as diffuse intensity which fills the rest of the area in the layer. The arrow indicates the incident beam direction for Figs. 4i, 6a-A, or 6b-C.

the circles A, B, and C containing many grains. On the other hand, OD patterns could be taken from individual grains after inserting small apertures (Figs. 9c-D and 9c-

E). These two OD patterns show the characteristic rectangle patterns in different orientations.

From the results presented in Figs. 8 and 9, it is clarified that the "disordered phase" contains small crystal grains in different orientations. The next thing to be performed is the determination of the unit cell size of the crystal lattice. In Fig. 10a, the intensity distribution on the 0th layer in the reciprocal space is schematically shown, where the two sets of rectangular diffraction configuration are drawn by open respectively full circles. For the further discussion in this report, they are named as reciprocal lattices I and II, respectively. The points indicated by broken circles are those which could be recognized as spots in the experimentally observed patterns, i.e., Figs. 4i, 6a-A, or 6b-C. The rotation axes of the series in Figs. 4, 6a, and 6b are marked by A, B, and C, respectively. The reciprocal space has the layer structure and it is assumed that the "disordered phase" does not give any diffraction spots between the layers. Therefore, the simplest way to describe the unit cell of the crystal lattice is to assume the two edges of the rectangle as the lattice vectors $\mathbf{a}^*$ and $\mathbf{b}^*$ as shown in Fig. 10a, respec-
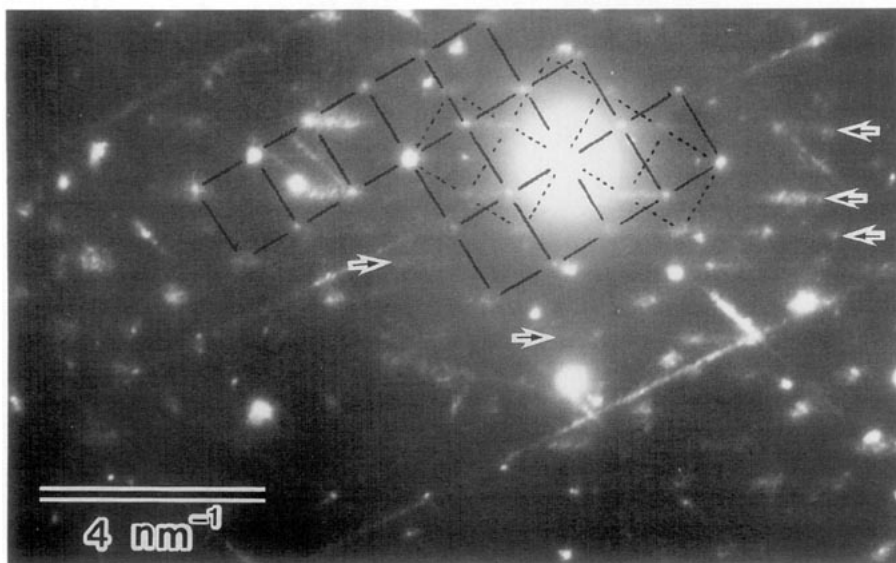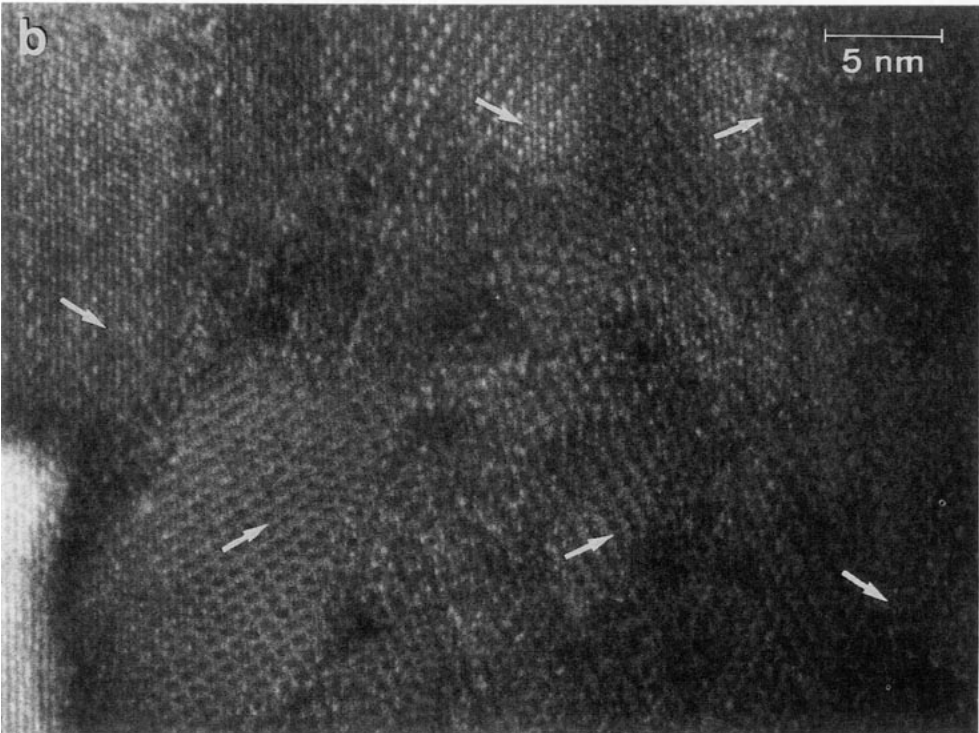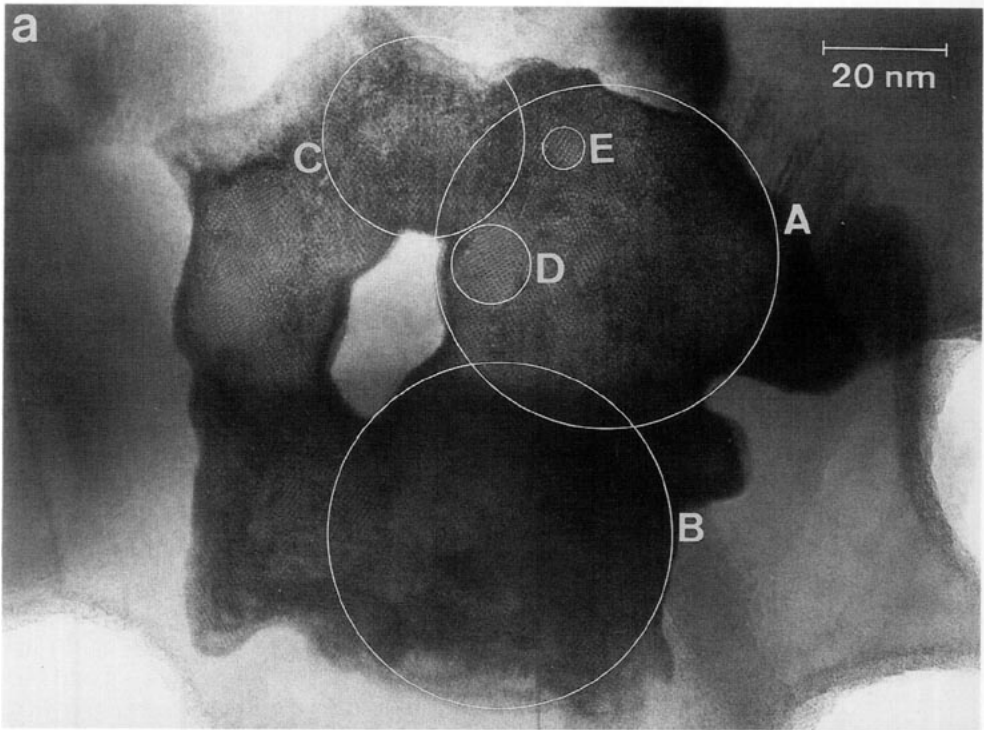

FIG. 8. Enlarged diffraction pattern of Fig 6a-B. Two sets of diffraction spots constituting rectangular nets (full or broken lines) are recognized. "Fine streaks" are marked by arrows.
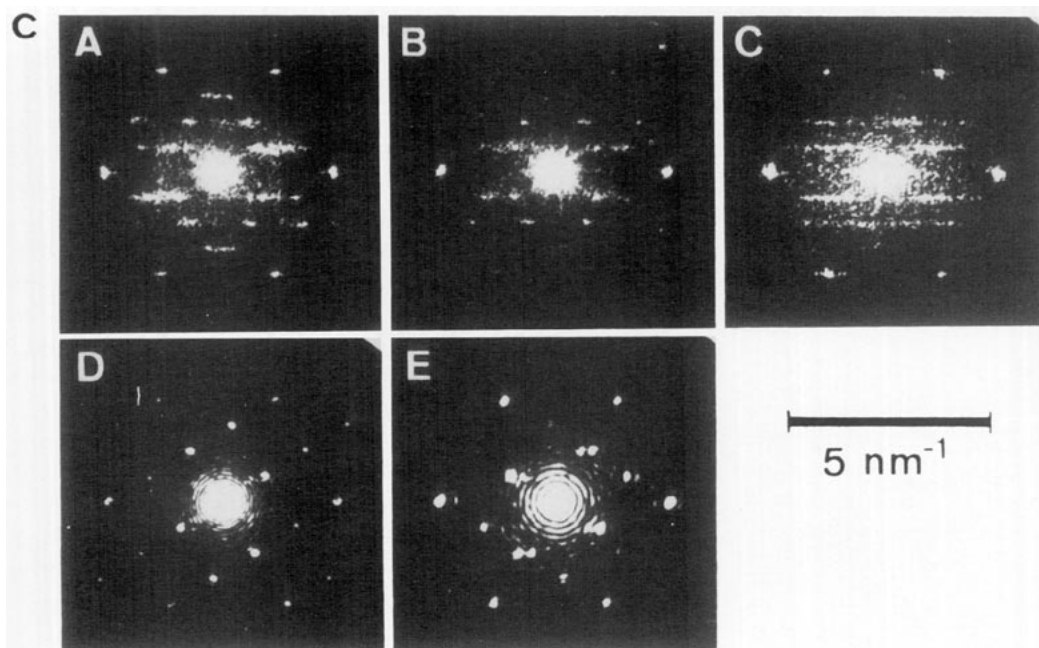
FIG. 9. High resolution micrograph of the "disordered phase" used in Fig. 6, where the observation was performed under a condition giving the diffraction in Fig. 6a-A. The "disordered phase" is an assembly of small crystal grains. (b) Enlarged image of (a) from the area marked by A. (c) Laser optical diffractograms from A to E of (a), respectively.

tively. After the detailed measurement of spot positions in Fig. 4i, the crystal lattice of the "disordered phase" used in Fig. 4 has the reciprocal lattice parameters, $a^* = 1.18$ nm^{-1} and $b^* = 1.49$ nm^{-1}.

In order to obtain information on the c^* vector of the crystal lattice, the rotation series of Fig. 4 are analyzed in detail. For the analyses, only the patterns containing relatively spotty intensity maxima on the streaks are treated, i.e., Figs. 4a, 4b, 4c, and 4h. In this case, the rotation axis is the one marked by A in Fig. 10a, which corresponds to the shorter edge of the rectangular reciprocal net (a^*-direction) of lattice I. In principle, two cases can be listed for the orientation of the rotation axis in reciprocal space: (1) a^* of lattice I and (2) $2a^* + 3b^*$ of lattice II. Since the periodicities along the streaks in Figs. 4a, 4b, and 4c are the same as the a^* spacing of the crystal, the a^*-direction of lattice I is defined as the rotation axis. In Fig. 10b, the cross section of the reciprocal lattice I containing (000) after the observation along the axis A of Fig. 10a is shown. Therefore, a^* vector is perpendicular to the plane of this figure. The shadowed lines marked by 0th, 1st and 2nd correspond to the layers in Fig. 7. Lines denoted by 4a, 4b, 4c, and 4h, are the cross section of the Ewald spheres for Figs. 4a, 4b, 4c, and 4h, respectively. The encircled dot is (000), and the open circles correspond to the observed spots on the plane perpendicular to the rotation axis. From the data presented here, the unit cell in the reciprocal space can be selected as the rectangle shown by thick broken lines. Therefore, the c^* vector is perpendicular to the layer and $c^* = 2.83$ nm^{-1}. In conclusion, an orthorhombic reciprocal lattice with $a^* = 1.18$ nm^{-1}, $b^* = 1.49$ nm^{-1} and $c^* = 2.83$ nm^{-1} is defined as one possible selection for the unknown crystal in the region of the "disordered phase." In the real space, $a = 0.85$ nm, $b = 0.67$ nm and $c = 0.35$ nm. The
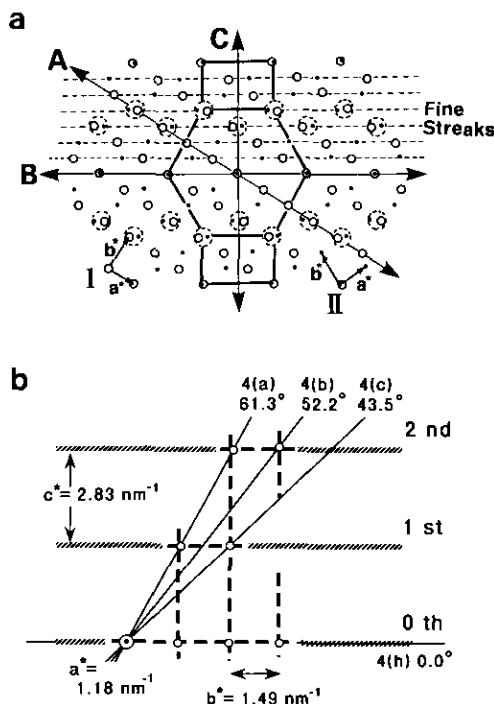
FIG. 10. (a) Schematic diffraction pattern near the center beam, which corresponds to Figs. 4i, 6a-A, or 6b-C. The pattern is a superposition of two reciprocal nets composed of open respectively full circles. By connecting the positions where two diffraction spots are nearly superimposed (broken circles), hexagonal configuration is recognized. The axes A, B, and C are the rotation axes used in Figs. 4, 6a, and 6b, respectively. (b) Schematic drawing of the rotation series of Fig. 4 observed along the rotation axis, A of (a). Ewald spheres of Figs. 4a, 4b, 4c, and 4h are indicated by lines with the rotation angles from 4h.

values of the lattice parameters differ by about several percent depending on the "disordered phase" investigated. Using this definition of the crystal lattice, the zone axis to obtain the high resolution image of Fig. 9 is [001] which is common for two crystal lattices.

3.3. Defects

In order to understand the origin of the intensity component other than the crystalline spots, i.e., "fine streaks" and diffuse

intensity, another high resolution image of the "disordered phase" was taken along [001] of the crystal lattice (Fig. 11a). For the discussion using this figure, the images are divided into five areas marked by A, B, C, D, and E. This "disordered phase" contains small crystal grains. A, B, C, and D show rectangular cross-fringe contrasts which indicate the crystal lattices projected along [001]. The a and b vectors in each area are shown in the figure. The lattices at A and B are rotated by 64° against each other, while they have parallel orientation at B and D. In the area marked by B, contrasts indicating planar defects are recognized (arrows) which are on {210}-planes. In C, the lattice fringe is very defective. The defect planes here are also on {210}. The OD pattern from C is presented as Fig. 11b. The pattern gives the "fine streaks" discussed above. Thus, it is clearly said that such a set of defects on {210} is the origin of the "fine streaks".

By contrast, the area marked by E in Fig. 11a, shows very weak contrast which is similar to that of amorphous material. This part surrounds a small crystalline grain. Probably, such part of the "disordered phase" contributes to the diffuse intensity which fills the layer in the reciprocal space. In addition, the crystalline lattices in the regions of "disordered phase" are randomly distorted. For example, in the image of Fig. 9, detailed measurement of the lattice fringes implied that the ratios of lattice parameters b/a slightly change from place to place. This is possibly due to a modulation of the concentration and/or internal stress introduced during the fast solidification from the vapor. Such distortion of the lattice may also be the origin of the diffuse intensity in the reciprocal space.

In order to investigate the crystal defects on {210} in detail, which contribute to the "fine streaks," images from the "disordered phase" used in Fig. 9 are magnified and presented as Figs. 12 and 13. They were observed along [001] of the crystal lattice. Figure 12 shows a planar defect (arrow A) and
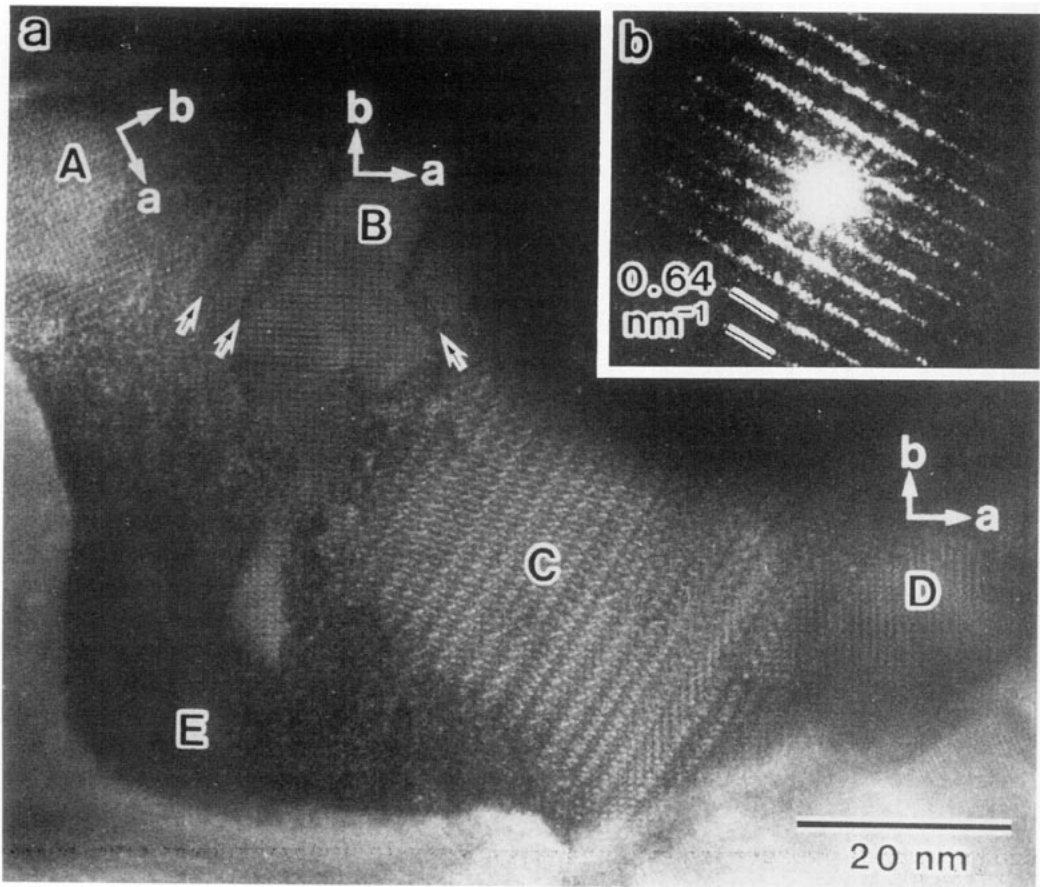
FIG. 11. (a) High resolution image observed along [001] of the crystal lattice. At the areas marked by *A*, *B*, *C*, and *D*, rectangular cross-fringe contrast indicating the unit cell is recognized. The unit cell vectors are shown. (b) Optical diffraction pattern from the area marked by *C* in (a). "Fine streaks" are seen.

a straight grain boundary (arrow *B*). The image contrast is that of a "distorted hexagon," and the rectangular net constructed from the relatively strong spots defines the unit cell. Figure 13 contains a set of straight grain boundaries indicated by thick lines, where rectangular net of the spots defined the unit cell.

In Fig. 12, the planar defect is on the (210)-plane, and the translation vector is $\frac{1}{4} \cdot [1\,2\,z]$; whereby the z-value is not known in this case. The periodicity of the "distorted hexagon" is not disturbed by the planar defects *A*, while, on the other hand, this defect offsets the lattice of the rectangular net. Thus

it is concluded that the rectangular net can be described as a superlattice structure of the basic "distorted hexagon" net. Consequently, the planar defect can be described as a defect of the superlattice and as an antiphase boundary of the basic "distorted hexagon."

At the grain boundary in Fig. 12, lattices marked by I and II are rotated against each other by 64°. The boundary planes have the index {210}, and the relatively strong spots of both adjacent grains coincide at the boundary plane. In the boundary region, a contrast defining kite-shape units can be recognized. In Fig. 13, a set of grain bound-
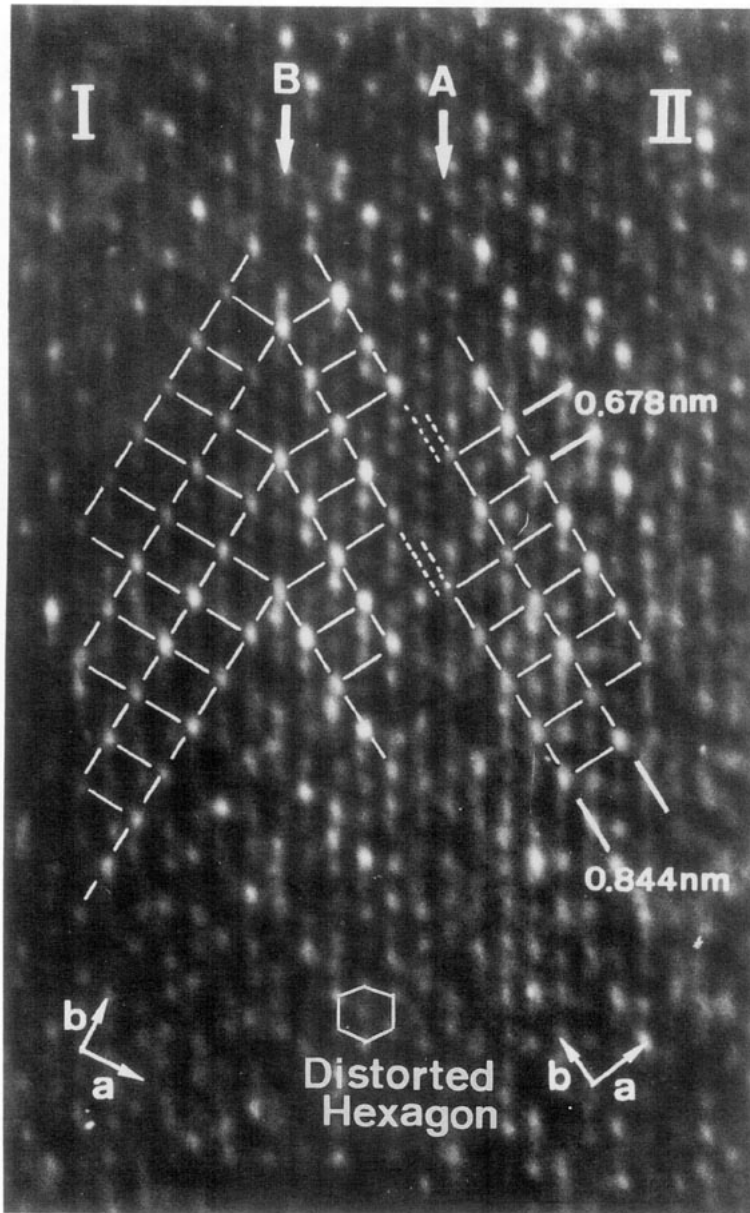
Fig. 12. A planar defect (arrow A) and a straight grain boundary (arrow B) in crystals observed along the c-axis. Rectangles constructed by brighter spots indicate unit cells. Lattice I is rotated 64° clockwise around the c-axis with respect to lattice II. Defect plane in both cases is {210}.

aries is visible. Crystal lattices having two different orientations are marked by I and II. The general structure of the boundary is the same as that in Fig. 12, while the rotation angle here deviates slightly from 64°. From the right to the left, the crystal domains change their orientation from I to II at the boundary A_1 which consists on the kite-shaped units described above. The orientation changes again from II to I at B_1, where
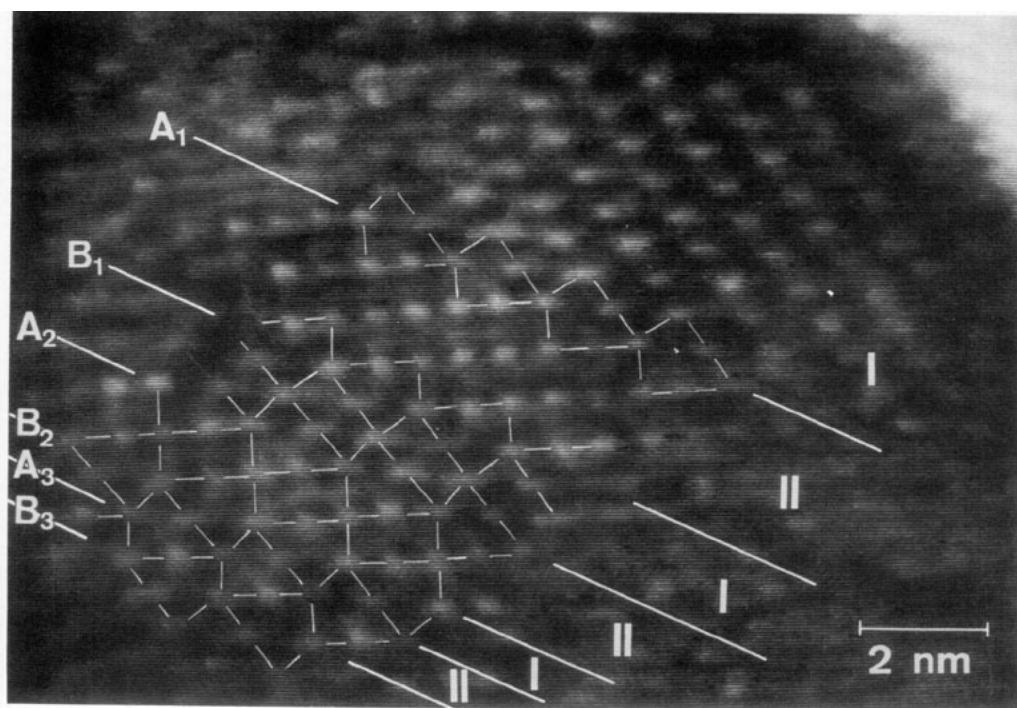
FIG. 13. Area with many grain boundaries. Image was copied from a TV screen. For detail, see text.

the orientation of the kites is opposite. The texture described here corresponds to a microtwin texture in other crystalline materials (cf., the superstructure in mullite, Figs. 6 and 7 in ref. (18)). Towards the left lower margin, the width of the domains is reduced. Finally, only the kite-shaped unit constitute the domains I and II (B_2 and B_3), and no rectangular contrast is present. This area thus represents a highly disordered (or defected) region in which the defects are arranged periodically.

4. Summary and Conclusions

From the electron microscopic evidence presented, it can be concluded that the region of the "disordered phase" are assemblies of small grains. Their germanium concentrations are about 30 ± 5 at.% assuming that they contain only Nb and Ge, while it is still unknown whether they are oxides or not. Some of the grains show a contrast similar to that of amorphous materials. The remaining grains are crystals with very many defects, which may have a new orthorhombic structure with $a = 0.85$ nm, $b = 0.67$ nm, and $c = 0.35$ nm.

For these crystalline grains, mainly two crystal orientations were observed which have their c-axis in common. Straight grain boundaries are parallel to {210}-planes. Planar defects observed in these grains are also on {210}-planes. These defects have been shown to disrupt the superlattice, but not the basic "distorted hexagon structure." Distortions of the lattice were also observed. Due to these features, the reciprocal space of one region of the "disordered phase" has a layer-type intensity distribution along the c*-axis. The layer contains spots, streaked intensity maxima, "fine streaks" and, possibly, planes of diffuse intensity. The first two features can be explained by the structure and defects of the crystalline grains. The "fine streaks" are due

to the planar defects and grain boundaries on {210}. The layers of diffuse intensity may be a contribution from the grains with contrast similar to that of amorphous materials and possibly also to the shape of small grains and to lattice distortions. The layered intensity distribution causes the streaked patterns obtained from observation along any direction of the electron beam.

The SAD technique using a small aperture has been successfully applied in the present investigation, aiming to clarify the structure of the "disordered phase" in Nb–Ge films. This method, combined with the nanodiffraction technique has provided information on the crystal structure of small grains in other materials such as the new high T_c oxide superconductors.

Acknowledgments

References

1. K. HIRAGA, D. SHINDO, M. HIRABAYASHI, M. KIKUCHI, AND Y. SYONO, *J. Electron. Microsc.* **36**, 261 (1987).
2. E. A. HEWAT, M. DUPUY, P. BORDET, J. J. CAPPONI, C. CHAILLOUT, J. L. HODEAU, AND M. MAREZIO, *Nature* **333**, 53 (1988).
3. S. AMELINCKX, G. VAN TENDELOO, J. VAN LANDUYT, AND H. W. ZANDBERGEN, *J. Less-Common Met.* **150**, 71 (1989).
4. W. SCHELB, *J. Mater. Sci.* **16**, 2575 (1981).
5. Y. KITANO, H.-U. NISSEN, R. WESSICKEN, D. YIN, AND W. SCHAUER, *J. Appl. Phys.* **58**, 1904 (1985).
6. V. M. PAN, V. I. LATYSHEVA, AND E. A. SHISHKIN, *in* "Physics and Metallurgy of Superconductors," (E. M. Savitskii, and V. V. Baron, Eds.), p. 179, Consultants Bureau, New York (1967).
7. A. B. HALLAK, E. H. HAMMOND, T. H. GEBALLE, AND R. B. ZUBECK, *IEEE Trans. Magn.* **MAG13**, 311 (1977).
8. J. L. JORDA, R. FLÜKIGER, *J. Less-Common Met.* **62**, 25 (1978).
9. A. G. CULLIS, J. M. POATE, AND L. R. TESTARDI, *Philos. Mag.* **36**, 1035 (1977).
10. S. PAÏDASSI, *Thin Solid Films* **69**, 69 (1980).
11. D. YIN, W. SCHAUER, AND F. WÜCHNER, *IEEE Trans. Magn.* **MAG19**, 276 (1983).
12. Y. KITANO, H.-U. NISSEN, W. SCHAUER, AND D. YIN, "Proc. 17th Internat. Conf. Low Temp. Phys.," Part 1, p. 615, Karlsruhe (1984).
13. M. STENZEL, Diploma thesis, Univ. Karlsruhe and Kernforschungszentrum Karlsruhe, Inst. für Tech. Phys., Karlsruhe, Germany (1985).
14. M. ARITA, Doctoral thesis, ETH-Zürich, No. 8288, Zürich, Switzerland (1987).
15. B. KREVET, W. SCHAUER, AND F. WÜCHNER, KfK Report 2579, Kernforschungszentrum Karlsruhe, Karlsruhe, Germany (1978).
16. M. KONRAD, KfK Report 3244, Kernforschungszentrum Karlsruhe, Karlsruhe, Germany (1981).
17. D. YIN AND W. SCHAUER, KfK Internal Report 03.05.02P01E, Kernforschungszentrum Karlsruhe, Karlsruhe, Germany (1982).
18. J. YLÄ-JÄÄSKI AND H.-U. NISSEN, *Phys. Chem. Miner.* **10**, 47 (1983).